

**PCCP**

Uptake of Water by an Acid-Base Nanoparticle: Theoretical and Experimental Studies of the Methanesulfonic Acid-Methylamine System

Journal:	<i>Physical Chemistry Chemical Physics</i>
Manuscript ID	CP-ART-06-2018-003634.R2
Article Type:	Paper
Date Submitted by the Author:	10-Aug-2018
Complete List of Authors:	Xu, Jing; University of California, Chemistry Perraud, Veronique; University of California, Chemistry Finlayson-Pitts, Barbara; University of California, Irvine, Department of Chemistry Gerber, Robert; The Hebrew University of Jerusalem , Chemistry; University of California, Irvine,

SCHOLARONE™
Manuscripts

1
2
3
4
5
6
7
8
9
10
11
12
13
14
15
16
17
18
19
20
21
22
23
24
25
26
27

Uptake of Water by an Acid-Base Nanoparticle: Theoretical and Experimental Studies of the Methanesulfonic Acid-Methylamine System

Jing Xu^a, Véronique Perraud,^a Barbara J. Finlayson-Pitts^a and R. Benny Gerber*^{a,b}*

^aDepartment of Chemistry
University of California, Irvine
Irvine, CA 92697, USA

^bInstitute of Chemistry, Fritz Haber Research Center
Hebrew University of Jerusalem
Jerusalem 91904, Israel

For submission to:

Physical Chemistry Chemical Physics

1 Abstract

2 The effect of water on the growth of dry nano-size acid-base particles is not yet known. In this
3 paper, we investigate the uptake of water by nano-size particles composed of methanesulfonic
4 acid (MSA) and methylamine (MA) using a combination of quantum chemical calculations and
5 laboratory experiments. Calculations were performed on the (MSA-MA)₄ cluster as the dry
6 nanoparticle model, which forms a pseudo-cubic structure, to which twelve water molecules
7 were added successively. Theoretical results show that the hydrated clusters (MSA-MA)₄-(H₂O)_n,
8 $n = 1$ to 12 are thermodynamically stable. In *ab initio* dynamic simulations, no loss of water or
9 significant changes of structure are seen for at least 10 picoseconds. In all the clusters studied,
10 most of water molecules lie on the face of the (MSA-MA)₄ initial dry unit, and water is found to
11 be incorporated inside the initial unit for n ranging from five to twelve. Sizes of hydrated clusters
12 exceed significantly those of the dry cluster only for $n \geq 6$. These theoretical results suggest that
13 dry MSA-MA clusters cannot dissociate in small quantities of water. Calculations of hydrated
14 cluster distributions at steady state show that the cluster compositions studied, with up to 12
15 water molecules, encompass all the hydrated clusters under the experimental conditions (RH ~
16 19%, 300 K). Experiments performed in a glass flow reactor showed no changes in size or
17 number concentration when particles formed from MSA-MA were subsequently exposed to
18 water vapor, in contrast to increases in both size and number when water was present *during*
19 particle formation. Thus, the results seem to imply for both experiment and theory that growth in
20 size of a particle due to uptake of water requires the previous presence of some level of hydration.
21 These results illustrate the importance for atmospheric models of understanding on a molecular
22 basis the mechanisms of particle formation in air.

23

1 Introduction

2 Atmospheric particles are well-known for their negative effects on climate^{1,2} and human health.³⁻
3 ⁵ Acid-base particles are a common class of atmospheric particles and have received increasing
4 attention.⁶⁻⁸ Sulphuric acid (H_2SO_4) has been identified as a key component in atmospheric
5 particles.⁹⁻¹¹ Numerous experimental studies have shown that bases, e.g., ammonia or amines,
6 can enhance new particle formation compared to the binary system $\text{H}_2\text{SO}_4\text{-H}_2\text{O}$,¹¹⁻¹⁶ in
7 agreement with theoretical calculations that acid-base clusters are more stable than hydrated
8 H_2SO_4 clusters.¹⁷⁻²⁵ In addition to well-known H_2SO_4 , methanesulfonic acid ($\text{CH}_3\text{S}(\text{O})(\text{O})\text{OH}$,
9 MSA) is another important sulfur-containing acid in the atmosphere.²⁶⁻³⁶ The concentrations of
10 gaseous MSA in the atmosphere are in the range of $\sim 10^5\text{-}10^7$ molecules cm^{-3} (corresponding to
11 10-100% of that of H_2SO_4),³⁶⁻³⁸ which can drive new particle formation (NPF) in air.³⁹ The
12 formation of particles involving MSA and ammonia/amines in the presence and absence of water
13 have been previously explored in laboratory studies,³⁹⁻⁴⁵ and corresponding quantum chemical
14 calculations on MSA-based clusters were also carried out.^{39-42,45-54} However, compared to
15 H_2SO_4 , the studies on MSA are still very limited.

16
17 There is a lot of evidence that the presence of water has a significant effect on NPF from both
18 MSA and H_2SO_4 .^{6,7,11-14,39-43,55-58} For example, laboratory measurements show that the formation
19 of MSA-amine particles are more efficient in the presence of water vapor, and particle number
20 concentrations and size distributions both increase as the relative humidity increases.³⁹⁻⁴³
21 Computational studies also suggest that the presence of water leads to a higher particle formation
22 rate compared to the dry case.^{59,60} Quantum chemical calculations indicate that water can
23 facilitate proton transfer from the acid to the base,^{18,20,46,47,60-65} stabilize the acid-base
24 clusters,^{17,18,22,47,64} and reduce the reaction barrier.⁶⁶ Most of these studies show the effect of
25 water in the initial step of NPF, while the role of water uptake on particles already present
26 remains uncertain.

27 Methylamine (CH_3NH_2 , MA) is an amine commonly found in the atmosphere.⁶⁷⁻⁶⁹ Earlier
28 studies demonstrated that MSA combines efficiently with MA to form nanoparticles,^{41,43,44} and
29 the structures of the corresponding nano-size low-energy anhydrous MSA-MA clusters were
30 reported in a previous study.⁴⁸ Inspired by this, the objectives in this paper can be described as
31 follows: (1) What is the effect of added water molecules on the size and other properties of dry
32 nanoparticles composed of MSA and MA? (2) Connected with this, what is the stability of the
33 MSA-MA nanoparticles with respect to the addition of water?

34 We report here a combined theoretical and experimental investigation of the uptake of water by
35 pre-existing MSA-MA nanoparticles. For the theoretical calculations, a cage-like $(\text{MSA-MA})_4$
36 cluster was chosen as the model of a nano-size acid-base particle. A previous study predicted that
37 this cluster has a very high thermodynamic and dynamic stability and can be seen as an
38 important intermediate in the formation and growth of MSA-MA particles.⁴⁸ Calculations

1 examine how this initial cluster behaves in presence of increasing numbers of water molecules
2 ranging from one to twelve, where the clusters are calculated using density functional theory and
3 *ab initio* molecular dynamics. Energetics, structures and dynamics of these hydrated clusters are
4 also reported. Experiments carried out in a glass flow reactor where MSA reacts with MA under
5 dry conditions, and subsequently exposed to water vapor are presented in support of the
6 calculations.

7

8 **Theoretical Methods**

9 The initial structures for the $(\text{MSA-MA})_4\text{-(H}_2\text{O)}_n$ ($n = 1$ to 12) clusters were obtained by
10 gradually adding water molecules to the stable cage-like $(\text{MSA-MA})_4$ anhydrous cluster. In
11 previous study,⁴⁸ more than three hundred initial structures of cluster composed of four MSA and
12 four MA were generated randomly using PACKMOL package. Upon optimization, the cage-like
13 $(\text{MSA-MA})_4$ still has the lowest energy among all local minima computed. The next lowest in
14 energy conformer is higher by 4.71 kcal/mol than the cage structure, and quickly converts to the
15 latter in room temperature molecular dynamics simulations. Hence, the cage-like $(\text{MSA-MA})_4$
16 can be seen as the global minimum, and is a reasonable model for this study. Because the 3-D
17 skeleton of the $(\text{MSA-MA})_4$ initial cluster looks like a cube, the probable locations of the added
18 water molecules we considered here are ‘on the face of’ or ‘inside’ the $(\text{MSA-MA})_4$ unit,
19 respectively. The geometry of the most stable $(\text{MSA-MA})_4$ unit defined from our previous study
20 was used as the starting anhydrous structure.⁴⁸ In order to consider possible local minima,
21 PACKMOL package was employed to generate initial structures. Optimization, frequency, and
22 energy calculations for these nanoclusters were performed using the BLYP-D^{70,71}/6-31+G(d)
23 method.^{72,73} In order to verify the credibility of the small basis set, more costly basis sets such as
24 aug-cc-pVDZ⁷⁴ and 6-311++G(3df, 3dp)⁷⁵ were used for our test calculations on three low-lying
25 isomers of the smallest cluster $(\text{MSA-MA})_4\text{-H}_2\text{O}$. The locations of water molecules in the three
26 isomers are 1) on the face of the $(\text{MSA-MA})_4$ cluster, binding with two deprotonated MSA
27 (MSA^-) and one protonated H^+MA ; 2) on the face of the $(\text{MSA-MA})_4$ cluster, binding with two
28 MSA^- ; and 3) inside of the $(\text{MSA-MA})_4$ unit, binding with two MSA^- , respectively. In addition,
29 the three isomers were also calculated using the B3LYP-D3^{71,76,77}/aug-cc-pVDZ method, which
30 has been tested on MSA-MA and is in agreement with MP2 and CCSD(T) results in a previous
31 study.⁴⁷ Figure S1 shows the corresponding structures and the relative energies of the three
32 isomers at the levels of BLYP-D/6-31+G(d), BLYP-D/aug-cc-pVDZ, BLYP-D/6-311++G(3df,
33 3dp) and B3LYP-D3/aug-cc-pVDZ. All the energies have been corrected with zero-point
34 energies. The test results showed similar structures and relative energies at the four levels of
35 theory. Hence, the less time-consuming BLYP-D/6-31+G(d) is considered to be sufficient to
36 predict qualitatively the lowest-energy isomer for the nano-size clusters investigated in the
37 present study. In order to compare the charge distributions of hydrated and anhydrous clusters,
38 natural bond orbital (NBO) analysis was used to calculate partial charges (δ).^{78,79}

1 Molecular dynamic (MD) simulations are usually used to verify the dynamic stability at various
2 temperatures. The dynamic stability we mean here is relevant to processes such as structural
3 rearrangements of the hydrated clusters and to proton transfer rates within these small particles,
4 which may yield different results compared to quantum chemical calculations performed at 0 K.
5 Hence, Born-Oppenheimer molecular dynamics (BOMD) simulations were carried out on each
6 hydrated cluster at $T = 300$ K for 10 picoseconds (ps) using the BLYP-D/6-31+G(d) potential
7 on-the-fly method. The time step used was 0.48 femtosecond (fs). All calculations in this paper
8 were performed using the Q-CHEM 4.3 program package.⁸⁰

9 In order to study the hydrate distribution, the simulations of steady-state concentrations of
10 clusters were performed using Atmospheric Cluster Dynamic Code (ACDC).⁸¹ We used (MSA-
11 MA)₄ and H₂O as the monomers to simulate the concentrations of hydrated clusters. For
12 matching the realistic experimental conditions, we assumed that the concentrations of (MSA-
13 MA)₄ and water were 10^6 and 10^{17} (RH=19%) molecules cm⁻³, respectively. Note that no
14 external sinks, e.g., coagulation scavenging or wall and dilution losses, were considered here.

15

16 Experimental Methods

17 Experiments were performed using a custom-built 1-m borosilicate glass aerosol flow reactor
18 described in detail elsewhere.^{42,43,82} The flow reactor was equipped with three fixed perforated
19 ring inlets at the upstream end and three perforated spoke inlets that are movable as a unit to
20 change the reaction time between the rings and spokes, and spokes and sampling tube. The six
21 ports allow the addition of reactants separately at different points (see Fig. S2). The sequence of
22 addition was the following: 10 L min⁻¹ of clean dry clean air was injected in the first ring (ring
23 A); MSA (~0.2 L min⁻¹) mixed in with 1.8 L min⁻¹ of air was added through the second ring (ring
24 B); MA (~0.17 L min⁻¹) mixed in with 0.83 L min⁻¹ of air was added through the third ring (ring
25 C) facing backward; 3 L min⁻¹ of air was added through the second spoke (spoke 2); no air flow
26 was introduced via the first or last spoke inlets (spoke 1 and 3 respectively). The total flow rate
27 under those conditions was 16 L min⁻¹ and the reaction times along the length of the reactor were
28 determined using a conversion factor of 0.132 s cm⁻¹ based upon previous measurements.⁸² All
29 flows were controlled by high-precision mass flow controllers (Alicat or MKS) and were
30 checked with a flow meter (Gilibrator 2, Sensidyne) prior to each experiment. For experiments
31 performed under humid conditions (RH 18-19%), water vapor generated by passing 3 L min⁻¹ of
32 air through a bubbler maintain at room temperature was added either through the second spoke
33 (replacing the 3 L min⁻¹ of dry air), i.e., *after* the formation of the MSA-MA particles; or through
34 the first ring (ring A), i.e., with MSA reacting with MA and water *at the same time* (adjustment
35 of the air flow was then made to maintained a total of 10 L min⁻¹ through the ring). For all
36 experiments performed, spoke 2 was located 62 cm downstream from ring B, giving a reaction
37 time for MSA with MA of corresponding to a reaction time of ~8.2 s (taking ring B as $t = 0$ s)

1 before water was added at the spokes. The air used throughout the experiments was dry clean air
2 generated from a purge air generator (Parker-Balston, model 75-62) which was further purified
3 using carbon/alumina media (Perma Pure, LLC) and a 0.1 μm filter (DIF-N70; Headline Filters).
4 In addition, the air introduced at the first ring (ring A; 10 L min^{-1} or 7 L min^{-1}) was also passed
5 through a cartridge containing phosphoric acid (ACS grade, EMD) coated glass beads to
6 minimize contaminant ammonia that might be present in purge air prior to its introduction into
7 the flow reactor. All experiments were performed at atmospheric pressure and 296 K. Particle
8 number concentrations and size distributions were measured using a moveable stainless steel
9 sampling line located inside the flow reactor. The interaction time for water added through the
10 spokes with the preformed MSA-MA particles was 5.7 s up to the entrance of the sampling line.

11 Methanesulfonic acid was generated in the gas phase by passing dry purge air over the pure
12 liquid (Sigma-Aldrich, $\geq 99\%$) maintained at room temperature in a glass trap. The concentration
13 of MSA exiting the trap was measured regularly by collecting the entire flow of MSA onto a
14 0.45 μm Durapore filter (Millex-HV) for 10 min and subsequent extraction with 10 mL of
15 nanopure water (18.2 $\text{m}\Omega\text{-cm}$; model 7146; Thermo Scientific, Barnstead). The extracts were
16 then analyzed by ultra performance liquid chromatography electrospray mass spectrometry
17 (Quattro Premier XE, Waters) using a multiple reaction monitoring method (MRM, transition
18 m/z 95 \Rightarrow m/z 80). The concentration of MSA from the trap was 427 ± 39 ppb (1 standard
19 deviation, calculated from multiple samples taken over time). The flow reactor was conditioned
20 with MSA for approximately two days prior to experiments to passivate the wall of the inlet and
21 the reactor.

22 Gas phase MA was generated using a commercially available permeation tube (VICI Metronics)
23 containing the pure liquid enclosed inside a U-shaped glass tube immersed in a water bath to
24 maintain the temperature at 293 K. Purge air at 0.17 L min^{-1} flowed through the glass tube to
25 generate gas phase MA. The concentration of MA was measured regularly by ion
26 chromatography (Dionex ICS 1100). Collection of the gas phase amine was performed using a
27 custom-made cation ion exchange resin⁸³ for 20 min at a flow rate of ~ 0.11 L min^{-1} and
28 subsequent extraction with 10 mL of the IC eluent (0.05 M oxalic acid in 18.2 $\text{m}\Omega\text{-cm}$ water).
29 The eluent was made every day by diluting a concentrated commercial oxalic acid solution (0.5
30 M, Fluka) with 18.2 $\text{m}\Omega\text{-cm}$ water. Three successive extractions of the same cartridge were
31 carried out and summed up to yield the total concentration produced by the permeation tube. No
32 quantifiable ammonia or other contaminant was observed from the MA permeation tube and the
33 concentration of MA measured out of the permeation tube was 122 ± 5 ppb (1 standard deviation
34 estimated from the analysis of 3 replicates).

35 The concentrations reported hereafter for both MSA and MA in the flow reactor are upper limits
36 as both compounds are sticky may be lost on the wall of the inlets and the reactor, even after
37 extensive conditioning. The relative humidity inside the flow tube was measured using a Vaisala

1 RH probe (HMT 838, Vaisala). Particle size distributions were measured at 13.9 s reaction time
2 relative to ring B. For experiments where H₂O was added at spoke 2, this time includes 8.2 s of
3 which particle form from MSA and MA, and 5.7 s of interaction time of the preformed particles
4 with water. A scanning mobility particle sizer (SMPS, 3936) equipped with a TSI 3080 classifier,
5 a nano-differential mobility analyzer (model 3085, TSI), a butanol-based condensation particle
6 counter (model 3776, TSI), a ²¹⁰Po neutralizer (NRD, model 2021) and a 0.071 cm impactor
7 nozzle was used for these measurements. Sheath air flow was 15 L min⁻¹ and the aerosol flow
8 was 1.5 L min⁻¹. The cut-off diameter under those conditions is stated to be 2.5 nm by the
9 manufacturer based on sucrose particles. In all experiments, the flow reactor was conditioned
10 with the last reactant added for 2 hours prior to making measurements.

11

12 **Results and discussion**

13 **Locations of water molecules**

14 The nano-size (MSA-MA)₄ cluster was first optimized at the level of BLYP-D/6-31+G(d). The
15 resulting structure is consistent with our previous study,⁴⁸ i.e., a closed cage-like structure
16 composed of four ion pairs (MSA⁻-H⁺MA), with an average bond length of the hydrogen bonds
17 is 1.81 Å (Fig. S3). Twelve water molecules were then added to the (MSA-MA)₄ cluster
18 sequentially. The most stable structures of (MSA-MA)₄-(H₂O)_n, *n* = 1 to 12 are shown in Figure
19 1.

20 Clusters with *n* = 1, 2, 5 and 11 are chosen as representative clusters and are shown in Figure 2.
21 There are two distinct types of structures, with subsets within each. In the first type, water
22 resides on the face of the cluster (Fig. 2a, b) while in the second, it is located inside (Fig. 2c,d).
23 Within the first type of structure, in the case of one water molecule (Fig. 2a), the water lies on
24 one face of the (MSA-MA)₄ initial anhydrous unit. Under those conditions, water breaks one
25 original hydrogen bond between MSA⁻ and H⁺MA, and forms three new hydrogen bonds with
26 two MSA⁻ and one H⁺MA. Due to the strong ion-dipole forces between the cation and water,
27 and the anion and water, H₂O becomes a strong bridge between the two ions, and no dissociation
28 takes place. As seen in Figure 2b, there are cases where two water molecules are located on the
29 same face. As in the case of one water (Fig. 2a), the two water molecules insert themselves
30 between two ion pairs on one face, and form a four-membered ring with two oxygen atoms of
31 MSA⁻. The addition of the second H₂O leads to a higher symmetry than for *n*=1, which is also
32 supported by the calculated free energies in Table 1 discussed in detail below.

33 In the second type of structure, water inserts itself inside the (MSA-MA)₄ initial unit. Fig. 2c
34 shows one water molecule inside the unit, bonding with two MSA⁻. Fig. 2d corresponds to two

1 water molecules inside the unit. In this latter case, besides binding with MSA^- and H^+MA , the
2 two water molecules located inside the unit connect with each other through one hydrogen bond.

3 Scheme 1 summarizes the different locations for water molecules, in which the sulfur and
4 nitrogen atoms of the dry cluster are used to define the six faces of the cluster. For $n = 1, 3$ and 4 ,
5 all the water molecules are located on separate faces of the $(\text{MSA-MA})_4$ initial unit, and belong
6 to the first type. For $n = 2$, the two water molecules lie on the same face. The $(\text{MSA-MA})_4$ -
7 $(\text{H}_2\text{O})_2$ cluster with the two water molecules located on separate faces exists as well, but it has
8 about 1 kcal/mol higher energy (with zero-point energy correction) than the structure with the
9 two water molecules located on the same face. From $n = 5$ to $n = 10$, there is always one water
10 inside the $(\text{MSA-MA})_4$ unit binding with two MSA^- , while other water molecules are located on
11 the faces of the unit. The water molecules on the faces also prefer to remain isolated (one water
12 molecule per face); the situation where the cluster has two water molecules on one face is not
13 observed until $n = 8$. For the case of $n = 11$ and 12 , a second water molecule is incorporated
14 inside the $(\text{MSA-MA})_4$ unit cell, i.e., the structure with the two internal water molecules has the
15 lowest energy.

16 In short, in $(\text{MSA-MA})_4(\text{H}_2\text{O})_n$, $n = 1$ to 12 , most of the absorbed water molecules are around
17 the initial $(\text{MSA-MA})_4$ unit; with 5 to 10 water molecules, there is one water molecule
18 incorporated inside the unit, and two water molecules that are internal for $n = 11$ and 12 .

19 **Thermodynamic stabilities**

20 In order to verify the thermodynamic stabilities of the $(\text{MSA-MA})_4(\text{H}_2\text{O})_n$, $n = 1$ to 12 clusters,
21 the dissociation energies corrected with zero-point energy and Gibbs free energies ($T = 298 \text{ K}$)
22 for the twelve systems described above were calculated at the BLYP-D/6-31+G(d) level. The
23 energies are listed in Table 1. We considered two possible paths. First, the clusters dissociate to
24 four MSA monomers, four MA monomers and water, i.e., $(\text{MSA-MA})_4(\text{H}_2\text{O})_n \rightarrow 4 \text{ MSA} + 4$
25 $\text{MA} + n \text{ H}_2\text{O}$. From Table 1, the dissociation energy and free energy of each system in this
26 reaction are quite high, i.e., 190.6 to 326.6 kcal/mol for ΔE and 98.80 to 128.6 kcal/mol for ΔG .
27 These positive values indicate that the dissociation process is highly endothermic. For the
28 anhydrous cluster $(\text{MSA-MA})_4$, the corresponding values are 176.8 kcal/mol for ΔE and 98.21
29 kcal/mol for ΔG respectively at the same level of theory. Considering $(\text{MSA-MA})_4$ is a very
30 stable cluster, the second dissociating pathway corresponding to the loss of water (dehydration),
31 i.e., $(\text{MSA-MA})_4(\text{H}_2\text{O})_n \rightarrow (\text{MSA-MA})_4 + n \text{ H}_2\text{O}$, was also calculated. Similar to the first path,
32 all the dissociation energies and Gibbs free energies (13.84 to 149.9 kcal/mol for ΔE and 0.58 to
33 30.37 kcal/mol for ΔG) are positive, and both of them increase with increasing number of water
34 molecules. Hence, based on these results, we found that $(\text{MSA-MA})_4(\text{H}_2\text{O})_n$ clusters are very
35 stable thermodynamically.

36 **Dynamic stabilities**

1 The dynamic stabilities of $(\text{MSA-MA})_4\text{-(H}_2\text{O)}_n$ clusters were examined by BOMD simulations
2 carried out at $T = 300$ K. Structures for each system taken at 10 ps from the dynamic simulations
3 are shown in Figure S4. Simulation results show that all the clusters keep the key skeleton
4 although the structural parameters change slightly. The locations of the water molecules that
5 were initially on faces or incorporated inside the unit do not change, but the interactions of
6 several water molecules changed under the influence of the temperature. Here, clusters with $n =$
7 2, 9, 11 and 12 were chosen as the representative structures for the discussion. Fig. 3a ($n = 2$) and
8 3b ($n = 9$) represent the two types of changes that occur when two water molecules are initially
9 located on the same face of the $(\text{MSA-MA})_4$ unit: in one case, the two water molecules form a
10 new hydrogen bond between them (Fig. 3a), and on the other, one of the water breaks the initial
11 hydrogen bond and now only connects with one MSA^- (Fig. 3b). For $n = 11$ (Fig. 3c) and $n = 12$
12 (Fig. 3d) clusters, the change occurs on the second internal water molecule: instead of initially
13 connecting with MSA^- or H^+MA , the second internal water molecule forms new hydrogen bonds
14 with other water molecules located on the faces. In general, $(\text{MSA-MA})_4\text{-(H}_2\text{O)}_n$, $n = 1$ to 12
15 clusters show good dynamic stability, and it is expected that at $T = 300$ K, water will still be
16 taken up by $(\text{MSA-MA})_4$ clusters.

17 **Charge distributions in the hydrated clusters**

18 In order to explore the effect of water on electronic properties, partial charges (δ) of $(\text{MSA-}$
19 $\text{MA})_4\text{-(H}_2\text{O)}_n$, $n = 1$ to 12 clusters were calculated using Natural Bond Orbital (NBO) analysis
20 (see Table S1). For the anhydrous cluster $(\text{MSA-MA})_4$, the charge of each MSA^- fragment is -
21 0.82 and it is 0.82 for each H^+MA fragment, which results from proton transfer from each MSA
22 to each MA. Upon addition of water, the partial charges of MSA^- and H^+MA fragments only
23 change slightly. The biggest charge difference is 0.04 for MSA^- ($n = 7$) and 0.06 for H^+MA ($n =$
24 9, 10, 12). The charge of each water lying on the face of the $(\text{MSA-MA})_4$ unit is small, but
25 positive ($\delta = 0.00\sim 0.04$). However, the internal water molecules are very different. For the
26 clusters with one internal water ($n = 5$ to 10), the charge of the internal water molecule is
27 negative except for $n = 10$. With increasing numbers of water molecules, the negative charge of
28 the internal water gradually increases until it becomes positive ($\delta = -0.06$ for $n = 5$ and $\delta =$
29 0.01 for $n = 10$). When there are two internal water molecules in the $(\text{MSA-MA})_4$ cluster ($n = 11$
30 and 12), both positive and negative charges on the internal water molecules exist. Based on the
31 partial charge of each water molecule, the water located on the faces of the $(\text{MSA-MA})_4$ unit has
32 a positive charge and acts as an electron donor like MA, and the internal water molecules which
33 have a negative charge act as an electron acceptor like MSA. Hence, through considering the
34 total charges of all the water molecules in each system, it can be seen that water mainly plays a
35 role as an electron donor ($\delta_{\text{total}} = 0.01\sim 0.17$), and the only case where water acts as an electron
36 acceptor is for $n = 5$ ($\delta_{\text{total}} = -0.02$).

37 **Effect of hydration on sizes**

1 The effects of water on the key skeleton and the size of the hydrated clusters were also
2 investigated. In order to examine quantitative changes in the key (MSA-MA)₄ skeleton, the root-
3 mean-square deviation (RMSD) of the geometry of the (MSA-MA)₄ unit in each hydrated cluster
4 was calculated. Figure S5a represents the RMSD values of the whole (MSA-MA)₄ unit (in black)
5 and the same units without all the CH₃ groups (in red). When only one water molecule is added,
6 the change in geometry of the (MSA-MA)₄ cluster is small, and the RMSD value is 0.5.
7 However, the differences increase with increasing numbers of water molecules. The RMSD
8 value is about 0.8 for $n = 2$ to 8 and 1.3 for $n = 8$ to 12. When the rotation of CH₃ groups is not
9 considered, similar trends were also obtained (red data points in Fig. S5a).

10 In order to directly observe a change, the geometries of the (MSA-MA)₄ unit from all the
11 systems described were overlaid as shown in Figure S5b. It clearly shows that every fragment
12 moves, and these changes may also affect the sizes of each cluster. Scheme 2a shows the lengths
13 of hydrated and anhydrous (MSA-MA)₄ clusters in X, Y and Z directions, and the calculated
14 percentage change (%) of sizes from anhydrous (MSA-MA)₄ are shown in Scheme 2b. When $n =$
15 1 and 2, the sizes of clusters in three directions do not change except for $n = 2$, a change in size is
16 noted in the Y direction (about -17%). From $n = 3$ to $n = 5$, all the sizes begin to decrease and the
17 cluster with $n = 5$ has the smallest sizes (-19% for X, -23% for Y and -12% for Z). Then, when
18 more water molecules are added ($n = 6$ to 12), the size of the clusters increases and the biggest
19 increase is about 29% for $n = 11$ in the X direction. However, the final sizes at $n = 12$ increases
20 are 17 % for X, 16% for Y and 13% for Z. In summary, the addition of water does not change the
21 sizes of the hydrated clusters very much, and in fact, the sizes decrease for $n = 3, 4$ and 5.

22 Hydrate distributions

23 In order to estimate the distribution of hydrated clusters under realistic experimental conditions,
24 the concentrations of each cluster in steady state were simulated using the ACDC code. Figure 4a
25 shows the hydrate distributions of the clusters from $n = 0$ to $n = 12$ at 19% RH. From these
26 results, the order of populations is $n = 7$ ($\approx 59\%$) $\gg n = 4$ ($\approx 11\%$) $> n = 0$ ($\approx 10\%$) $> n = 2$
27 ($\approx 7\%$) $> n = 3$ ($\approx 6\%$) $> n = 6$ ($\approx 5\%$) $> n = 5/9$ ($\approx 1\%$) $> n = 1/8/10/11/12$ ($\approx 0\%$). It is clear that the
28 hydrated cluster with seven water molecules dominates, and its concentration is much higher
29 than the others. This is also supported by the evaporation rates of the hydrated clusters from a
30 single water evaporation pathway shown in Figure 4b. The difference of evaporation rates
31 between $n = 7$ and $n = 8$ is four orders of magnitudes, which means that the $n = 8$ cluster easily
32 evaporates back to the $n = 7$ cluster. A similar situation exists for $n = 1, 5, 10$. These clusters are
33 also likely to lose one water molecule. The hydrated cluster distributions at RH = 19% and 300 K
34 shows that clusters with $n > 12$ water are not significantly present. Therefore, the clusters studied
35 in this paper, ranging from $n = 1$ up to $n = 12$, describe all the hydrated clusters that are relevant.

36 Experimental results

1 Experiments performed on this system are consistent with the results from quantum calculations
2 described above. Figure 5a shows the size distribution from the reaction of 6.9 ppb MSA (1.7
3 $\times 10^{11}$ molecules cm^{-3}) with 1.6 ppb MA (3.9×10^{10} molecules cm^{-3}) under dry and humid
4 conditions where H_2O is added at a reaction time of 8.2 s *after* the formation of the MSA-MA
5 particles. Under these conditions of excess MSA, the lifetime of MA is calculated to be ~ 50 ms,
6 assuming a diffusion-controlled reaction. Thus, the 8.2 s of reaction time before water is added is
7 more than sufficient for the MSA-MA reaction to be brought to completion. Under this
8 configuration, no increase of detectable particles nor size change was observed at 19% RH ($[\text{H}_2\text{O}]$
9 $= 1.5 \times 10^{17}$ molecules cm^{-3}) as reported in Table 2. Although the experiments were conducted
10 with much more water than the theoretical calculations due to experimental constraints, the
11 experiments show that the small stable (MSA-MA) particles are not impacted by the presence of
12 water in agreement with the theoretical calculations presented in this study.

13 The absence of a deliquescence effect for the small systems studied here (~ 1 nm size for the
14 theoretical calculations and ~ 3 nm for the experiments at a relative humidity of 19%) is not
15 surprising. To the best of our knowledge, the deliquescence relative humidity (DRH) for the
16 MSA-MA salt has not been reported, but previous studies have shown that sodium
17 methanesulfonate deliquesced at about 70%^{84,85} (deliquescence relative humidity, DRH) while
18 ammonium methanesulfonate showed a continuous uptake of water.⁸⁴ However, those
19 measurements were all performed on ~ 1 μm particles deposited on a substrate, corresponding to
20 a macroscopic thermodynamic bulk system. This may not hold for the small nanosize particles
21 investigated here. Indeed, previous studies on hygroscopic growth and deliquescence for NaCl
22 and $(\text{NH}_4)_2\text{SO}_4$ nanoparticles showed that at 100 nm, the DRH is not very different than that of
23 the bulk value, but as the diameter of the particles approached only a few nm (8 – 15 nm), the
24 relative humidity at which the particle deliquesced became systematically higher. In small
25 nanosize systems, a large fraction of the molecules are on the surface rather than in the bulk and
26 thus the surface energy becomes a significant term in the total free energy of the particle.

27 In a separate set of experiments, however, where water was introduced upstream (ring A, Fig. 5b)
28 so that it was present *during* particle formation from MSA and MA, a very large increase of
29 particles was observed (10 times more particles were detected) compared to the dry case. The
30 particles were observed to be much larger as well, with a geometric mean diameter of 6.5 nm
31 compared to ~ 4 nm under dry conditions. Those results agree with our previous
32 observations,^{41,43} and indicate that water plays a central role in particle formation and growth in
33 this system when all the reactants are present *at the same time*, despite the fact that the MSA
34 reaction with water alone is not efficient. (A control experiment showed that less than 1 particle
35 cm^{-3} was measured by the CPC for the reaction of MSA (ring B, 5.3 ppb) with H_2O (ring A, 19%
36 RH) in absence of MA, suggesting that the large number of particles is due to the presence of
37 both the amine and water together.)

1 From a theoretical point of view, when 4 MSA, 4 MA and for example one water molecule
2 interact *at the same time*, low energy level structures include ‘unclosed’ clusters. These clusters,
3 as the one presented in Fig. S6, have a lot more opportunities to form hydrogen bonds with other
4 species providing hooks to growth the initial cluster to larger sizes, consistent with the
5 experimental observations.

6 The theoretical calculations cannot exactly replicate the conditions used for the experiments.
7 The smallest particles size that can be detected and measured using the SMPS is 2.5 nm, which is
8 much larger than the clusters calculated here. The time scales studied experimentally are also
9 much larger than that can be addressed theoretically. Where interesting comparisons can be made,
10 we investigated the connections between water uptake and increasing size, or in other words
11 particle growth: The 1 nm theoretical model cluster can take up water without significant
12 increase in size up to about $n \geq 6$. Beyond that size, the size of the particle continues to grow,
13 and the increase becomes about 30% for $n=11$. In the experiment, there is no significant uptake
14 of water for the dry particles subsequently exposed to water vapor (19% RH), but for the
15 particles produced with water vapor *at the same time* as the reactants, the size increases
16 substantially compared to the dry case. Note that our experimental conditions had lower water
17 vapor concentrations than found under many tropospheric conditions.

18

19 **Conclusions**

20 In this paper, the uptake of water by the MSA-MA nanoparticles via theoretical calculations and
21 experiments was studied. It was shown that these hydrated nano-size clusters are
22 thermodynamically stable at the level of BLYP-D/6-31+G(d). Loss of water and significant
23 changes of structure do not take place for at least 10 ps throughout *ab initio* dynamic
24 simulations. In the hydrated clusters, most of water molecules lie on the face of the (MSA-MA)₄
25 initial dry unit, with water incorporated inside the initial unit when n ranges from five to twelve.
26 Charge distributions in hydrated and anhydrous clusters are not very different. Sizes of hydrated
27 clusters differ by less than +30% to -25% in any dimension compared to the dry clusters, and the
28 increased sizes are found when $n \geq 6$. From the hydrate distributions, the hydrated cluster with
29 $n = 7$ dominates at 19% RH. Furthermore, the computed cluster distribution shows that the range
30 of hydrated clusters studied, $n < 13$, encompasses all of the clusters present at significant
31 concentrations under these conditions. In the experiments, the concentrations and size
32 distributions of MSA-MA particles do not change when the particles formed under dry
33 conditions are subsequently exposed to water vapor corresponding to 18-19% RH. These results
34 suggest that the effect of water on new particle formation and growth from MSA reactions with
35 amines will be sensitive to whether water is present during the reaction, or added subsequently.
36 Water is always present in the troposphere at significant concentrations, but not always in
37 laboratory studies. Thus extrapolation of experiments under dry conditions to the atmosphere

1 should be carried out with caution. Note that the theoretical calculations we studied in this paper
2 focus on the small cluster with very limited numbers of water molecules. It will be very
3 interesting in future studies to address the cluster with bulk water to compute the water loss rate
4 by an approach based on Transition State Theory.

5

6 **Author information**

7 **Corresponding Authors**

8 *For theory, R.B.G.: E-mail benny@fh.huji.ac.il

9 *For experiments, B.J.F.-P.: E-mail bjfinlay@uci.edu, phone (949) 824-7670, fax (949) 824-
10 2420

11

12 **Acknowledgments**

13 The authors are grateful to the National Science Foundation (grant no. 1443140) for funding.
14 Computational resources are the Green-planet cluster at University of California, Irvine. The
15 authors thank the reviewer for pointing to us the dominant role of a specific cluster over a wide
16 range of RH values. We thank Dr. Nanna Myllys for her help in computing the hydrated cluster
17 distribution and in providing useful insights.

18

19

40 **References**

41 1 J. H. Seinfeld and S. N. Pandis, *Atmospheric Chemistry and Physics: From Air Pollution to*
42 *Climate Change*, Wiley-Interscience, Hoboken, N.J, 2 edition., 2006.

43 2 T. F. Stocker, D. Qin, G. K. Plattner, M. Tignor, S. K. Allen, J. Boschung, A. Nauels, Y. Xia, B.
44 Bex and B. M. Midgley, *IPCC, 2013: Climate Change 2013: The Physical Science Basis. Contribution of*
45 *Working Group I to the Fifth Assessment Report of the Intergovernmental Panel on Climate Change*,
46 Cambridge University Press, Cambridge, United Kingdom and New York, NY, USA, 2013.

47 3 C. A. Pope and D. W. Dockery, *J. Air Waste Manag. Assoc.* 1995, 2006, **56**, 709–742.

48 4 J. L. Mauderly and J. C. Chow, *Inhal. Toxicol.*, 2008, **20**, 257–288.

49 5 J. Lelieveld, J. S. Evans, M. Fnais, D. Giannadaki and A. Pozzer, *Nature*, 2015, **525**, 367–371.

50 6 B. J. Finlayson-Pitts and J. N. P. Jr, *Chemistry of the Upper and Lower Atmosphere: Theory,*
51 *Experiments, and Applications*, Academic Press, 1999.

- 1 7 R. Zhang, A. Khalizov, L. Wang, M. Hu and W. Xu, *Chem. Rev.*, 2012, **112**, 1957–2011.
- 2 8 S. T. Martin, *Chem. Rev.*, 2000, **100**, 3403–3454.
- 3 9 M. Kulmala, J. Kontkanen, H. Junninen, K. Lehtipalo, H. E. Manninen, T. Nieminen, T. Petäjä,
4 M. Sipilä, S. Schobesberger, P. Rantala, A. Franchin, T. Jokinen, E. Järvinen, M. Äijälä, J. Kangasluoma,
5 J. Hakala, P. P. Aalto, P. Paasonen, J. Mikkilä, J. Vanhanen, J. Aalto, H. Hakola, U. Makkonen, T.
6 Ruuskanen, R. L. Mauldin, J. Duplissy, H. Vehkamäki, J. Bäck, A. Kortelainen, I. Riipinen, T. Kurtén, M.
7 V. Johnston, J. N. Smith, M. Ehn, T. F. Mentel, K. E. J. Lehtinen, A. Laaksonen, V.-M. Kerminen and D.
8 R. Worsnop, *Science*, 2013, **339**, 943–946.
- 9 10 M. Sipilä, T. Berndt, T. Petäjä, D. Brus, J. Vanhanen, F. Stratmann, J. Patokoski, R. L. Mauldin,
10 A.-P. Hyvärinen, H. Lihavainen and M. Kulmala, *Science*, 2010, **327**, 1243–1246.
- 11 11 J. H. Zollner, W. A. Glasoe, B. Panta, K. K. Carlson, P. H. McMurry and D. R. Hanson, *Atmos.*
12 *Chem. Phys.*, 2012, **12**, 4399–4411.
- 13 12 T. Berndt, F. Stratmann, M. Sipilä, J. Vanhanen, T. Petäjä, J. Mikkilä, A. Grüner, G. Spindler, R.
14 Lee Mauldin III, J. Curtius, M. Kulmala and J. Heintzenberg, *Atmos. Chem. Phys.*, 2010, **10**, 7101–7116.
- 15 13 M. E. Erupe, A. A. Viggiano and S.-H. Lee, *Atmos. Chem. Phys.*, 2011, **11**, 4767–4775.
- 16 14 H. Yu, R. McGraw and S.-H. Lee, *Geophys. Res. Lett.*, 2012, **39**, L02807.
- 17 15 W. A. Glasoe, K. Volz, B. Panta, N. Freshour, R. Bachman, D. R. Hanson, P. H. McMurry and C.
18 Jen, *J. Geophys. Res. Atmospheres*, 2015, **120**, 2014JD022730.
- 19 16 J. Almeida, S. Schobesberger, A. Kürten, I. K. Ortega, O. Kupiainen-Määttä, A. P. Praplan, A.
20 Adamov, A. Amorim, F. Bianchi, M. Breitenlechner, A. David, J. Dommen, N. M. Donahue, A. Downard,
21 E. Dunne, J. Duplissy, S. Ehrhart, R. C. Flagan, A. Franchin, R. Guida, J. Hakala, A. Hansel, M. Heinritzi,
22 H. Henschel, T. Jokinen, H. Junninen, M. Kajos, J. Kangasluoma, H. Keskinen, A. Kupc, T. Kurtén, A. N.
23 Kvashin, A. Laaksonen, K. Lehtipalo, M. Leiminger, J. Leppä, V. Loukonen, V. Makhmutov, S. Mathot,
24 M. J. McGrath, T. Nieminen, T. Olenius, A. Onnela, T. Petäjä, F. Riccobono, I. Riipinen, M. Rissanen, L.
25 Rondo, T. Ruuskanen, F. D. Santos, N. Sarnela, S. Schallhart, R. Schnitzhofer, J. H. Seinfeld, M. Simon,
26 M. Sipilä, Y. Stozhkov, F. Stratmann, A. Tomé, J. Tröstl, G. Tsagkogeorgas, P. Vaattovaara, Y. Viisanen,
27 A. Virtanen, A. Vrtala, P. E. Wagner, E. Weingartner, H. Wex, C. Williamson, D. Wimmer, P. Ye, T. Yli-
28 Juuti, K. S. Carslaw, M. Kulmala, J. Curtius, U. Baltensperger, D. R. Worsnop, H. Vehkamäki and J.
29 Kirkby, *Nature*, 2013, **502**, 359–363.
- 30 17 T. Kurtén, L. Torpo, C.-G. Ding, H. Vehkamäki, M. R. Sundberg, K. Laasonen and M. Kulmala,
31 *J. Geophys. Res. Atmospheres*, 2007, **112**, D04210.
- 32 18 J. C. Ianni and A. R. Bandy, *J. Phys. Chem. A*, 1999, **103**, 2801–2811.
- 33 19 A. B. Nadykto, F. Yu, M. V. Jakovleva, J. Herb and Y. Xu, *Entropy*, 2011, **13**, 554–569.
- 34 20 H. Henschel, T. Kurtén and H. Vehkamäki, *J. Phys. Chem. A*, 2016, **120**, 1886–1896.
- 35 21 V. Loukonen, T. Kurtén, I. K. Ortega, H. Vehkamäki, A. A. H. Pádua, K. Sellegri and M.
36 Kulmala, *Atmos. Chem. Phys.*, 2010, **10**, 4961–4974.
- 37 22 J. W. DePalma, D. J. Doren and M. V. Johnston, *J. Phys. Chem. A*, 2014, **118**, 5464–5473.

- 1 23 D. J. Bustos, B. Temelso and G. C. Shields, *J. Phys. Chem. A*, 2014, **118**, 7430–7441.
- 2 24 K. E. Anderson, J. I. Siepmann, P. H. McMurry and J. VandeVondele, *J. Am. Chem. Soc.*, 2008,
3 **130**, 14144–14147.
- 4 25 D. S. Lambrecht, L. McCaslin, S. S. Xantheas, E. Epifanovsky and M. Head-Gordon, *Mol. Phys.*,
5 2012, **110**, 2513–2521.
- 6 26 S. M. Kreidenweis and J. H. Seinfeld, *Atmospheric Environ. 1967*, 1988, **22**, 283–296.
- 7 27 M. C. Facchini, S. Decesari, M. Rinaldi, C. Carbone, E. Finessi, M. Mircea, S. Fuzzi, F. Moretti,
8 E. Tagliavini, D. Ceburnis and C. D. O’Dowd, *Environ. Sci. Technol.*, 2008, **42**, 9116–9121.
- 9 28 R. J. Hopkins, Y. Desyaterik, A. V. Tivanski, R. A. Zaveri, C. M. Berkowitz, T. Tylliszczak, M. K.
10 Gilles and A. Laskin, *J. Geophys. Res. Atmospheres*, 2008, **113**, D04209.
- 11 29 B. E. Wyslouzil, J. H. Seinfeld and R. C. Flagan, *J. Chem. Phys.*, 1991, **94**, 6827–6841.
- 12 30 B. E. Wyslouzil, J. H. Seinfeld, R. C. Flagan and K. Okuyama, *J. Chem. Phys.*, 1991, **94**, 6842–
13 6850.
- 14 31 S. M. Kreidenweis, R. C. Flagan, J. H. Seinfeld and K. Okuyama, *J. Aerosol Sci.*, 1989, **20**, 585–
15 607.
- 16 32 V.-M. Kerminen, M. Aurela, R. E. Hillamo and A. Virkkula, *Tellus B Chem. Phys. Meteorol.*,
17 1997, **49**, 159–171.
- 18 33 V. Perraud, J. R. Horne, A. S. Martinez, J. Kalinowski, S. Meinardi, M. L. Dawson, L. M.
19 Wingen, D. Dabdub, D. R. Blake, R. B. Gerber and B. J. Finlayson-Pitts, *Proc. Natl. Acad. Sci.*, 2015,
20 **112**, 13514–13519.
- 21 34 A. Sorooshian, L. T. Padró, A. Nenes, G. Feingold, A. McComiskey, S. P. Hersey, H. Gates, H.
22 H. Jonsson, S. D. Miller, G. L. Stephens, R. C. Flagan and J. H. Seinfeld, *Glob. Biogeochem. Cycles*,
23 2009, **23**, GB4007.
- 24 35 C. J. Gaston, K. A. Pratt, X. Qin and K. A. Prather, *Environ. Sci. Technol.*, 2010, **44**, 1566–1572.
- 25 36 H. Bardouki, H. Berresheim, M. Vrekoussis, J. Sciare, G. Kouvarakis, K. Oikonomou, J.
26 Schneider and N. Mihalopoulos, *Atmos. Chem. Phys.*, 2003, **3**, 1871–1886.
- 27 37 Berresheim H., Elste T., Tremmel H. G., Allen A. G., Hansson H.-C., Rosman K., Dal Maso M.,
28 Mäkelä J. M., Kulmala M. and O’Dowd C. D., *J. Geophys. Res. Atmospheres*, 2002, PAR 5-1.
- 29 38 F. L. Eisele and D. J. Tanner, *J. Geophys. Res. Atmospheres*, 1993, **98**, 9001–9010.
- 30 39 M. L. Dawson, M. E. Varner, V. Perraud, M. J. Ezell, R. B. Gerber and B. J. Finlayson-Pitts,
31 *Proc. Natl. Acad. Sci.*, 2012, **109**, 18719–18724.
- 32 40 H. Chen, M. J. Ezell, K. D. Arquero, M. E. Varner, M. L. Dawson, R. B. Gerber and B. J.
33 Finlayson-Pitts, *Phys. Chem. Chem. Phys.*, 2015, **17**, 13699–13709.
- 34 41 H. Chen, M. E. Varner, R. B. Gerber and B. J. Finlayson-Pitts, *J. Phys. Chem. B*, 2016, **120**,
35 1526–1536.

- 1 42 K. D. Arquero, J. Xu, R. B. Gerber and B. J. Finlayson-Pitts, *Phys. Chem. Chem. Phys.*, 2017, **19**,
2 28286–28301.
- 3 43 K. D. Arquero, R. B. Gerber and B. J. Finlayson-Pitts, *Environ. Sci. Technol.*, 2017, **51**, 2124–
4 2130.
- 5 44 H. Chen and B. J. Finlayson-Pitts, *Environ. Sci. Technol.*, 2017, **51**, 243–252.
- 6 45 M. L. Dawson, M. E. Varner, V. Perraud, M. J. Ezell, J. Wilson, A. Zelenyuk, R. B. Gerber and B.
7 J. Finlayson-Pitts, *J. Phys. Chem. C*, 2014, **118**, 29431–29440.
- 8 46 S. Li, L. Zhang, W. Qin and F.-M. Tao, *Chem. Phys. Lett.*, 2007, **447**, 33–38.
- 9 47 J. Xu, B. J. Finlayson-Pitts and R. B. Gerber, *J. Phys. Chem. A*, 2017, **121**, 2377–2385.
- 10 48 J. Xu, B. J. Finlayson-Pitts and R. B. Gerber, *Phys. Chem. Chem. Phys.*, 2017, **19**, 31949–31957.
- 11 49 N. Bork, J. Elm, T. Olenius and H. Vehkamäki, *Atmos. Chem. Phys.*, 2014, **14**, 12023–12030.
- 12 50 H. Zhao, X. Jiang and L. Du, *Chemosphere*, 2017, **174**, 689–699.
- 13 51 M. Kumar and J. S. Francisco, *Proc. Natl. Acad. Sci.*, 2017, **114**, 12401–12406.
- 14 52 L. Wang, *J. Phys. Chem. A*, 2007, **111**, 3642–3651.
- 15 53 S.-K. Miao, S. Jiang, X.-Q. Peng, Y.-R. Liu, Y.-J. Feng, Y.-B. Wang, F. Zhao, T. Huang and W.
16 Huang, *RSC Adv.*, 2018, **8**, 3250–3263.
- 17 54 A. Givan, A. Loewenschuss and C. J. Nielsen, *J. Mol. Struct.*, 2005, **748**, 77–90.
- 18 55 T. Berndt, M. Sipilä, F. Stratmann, T. Petäjä, J. Vanhanen, J. Mikkilä, J. Patokoski, R. Taipale, R.
19 L. Mauldin III and M. Kulmala, *Atmos Chem Phys*, 2014, **14**, 751–764.
- 20 56 M. Kulmala, H. Vehkamäki, T. Petäjä, M. Dal Maso, A. Lauri, V.-M. Kerminen, W. Birmili and
21 P. H. McMurry, *J. Aerosol Sci.*, 2004, **35**, 143–176.
- 22 57 D. G. Imre, J. Xu, I. N. Tang and R. McGraw, *J. Phys. Chem. A*, 1997, **101**, 4191–4195.
- 23 58 I. K. Ortega, O. Kupiainen, T. Kurtén, T. Olenius, O. Wilkman, M. J. McGrath, V. Loukonen and
24 H. Vehkamäki, *Atmos. Chem. Phys.*, 2012, **12**, 225–235.
- 25 59 H. Henschel, T. Kurtén and H. Vehkamäki, *J. Phys. Chem. A*, 2016, **120**, 1886–1896.
- 26 60 N. T. Tsona, H. Henschel, N. Bork, V. Loukonen and H. Vehkamäki, *J. Phys. Chem. A*, 2015,
27 **119**, 9670–9679.
- 28 61 H. Henschel, J. C. A. Navarro, T. Yli-Juuti, O. Kupiainen-Määttä, T. Olenius, I. K. Ortega, S. L.
29 Clegg, T. Kurtén, I. Riipinen and H. Vehkamäki, *J. Phys. Chem. A*, 2014, **118**, 2599–2611.
- 30 62 K. H. Weber, Q. Liu and F.-M. Tao, *J. Phys. Chem. A*, 2014, **118**, 1451–1468.
- 31 63 X.-Q. Peng, T. Huang, S.-K. Miao, J. Chen, H. Wen, Y.-J. Feng, Y. Hong, C.-Y. Wang and W.
32 Huang, *RSC Adv.*, 2016, **6**, 46582–46593.

- 1 64 S.-S. Lv, S.-K. Miao, Y. Ma, M.-M. Zhang, Y. Wen, C.-Y. Wang, Y.-P. Zhu and W. Huang, *J.*
2 *Phys. Chem. A*, 2015, **119**, 8657–8666.
- 3 65 L. J. Larson, A. Largent and F.-M. Tao, *J. Phys. Chem. A*, 1999, **103**, 6786–6792.
- 4 66 L. J. Larson, M. Kuno and F.-M. Tao, *J. Chem. Phys.*, 2000, **112**, 8830–8838.
- 5 67 X. Ge, A. S. Wexler and S. L. Clegg, *Atmos. Environ.*, 2011, **45**, 524–546.
- 6 68 Y. You, V. P. Kanawade, J. A. de Gouw, A. B. Guenther, S. Madronich, M. R. Sierra-Hernández,
7 M. Lawler, J. N. Smith, S. Takahama, G. Ruggieri, A. Koss, K. Olson, K. Baumann, R. J. Weber, A.
8 Nenes, H. Guo, E. S. Edgerton, L. Porcelli, W. H. Brune, A. H. Goldstein and S.-H. Lee, *Atmos. Chem.*
9 *Phys.*, 2014, **14**, 12181–12194.
- 10 69 I.-H. Chang, C.-G. Lee and D. S. Lee, *Anal. Chem.*, 2003, **75**, 6141–6146.
- 11 70 C. Lee, W. Yang and R. G. Parr, *Phys. Rev. B*, 1988, **37**, 785–789.
- 12 71 S. Grimme, J. Antony, S. Ehrlich and H. Krieg, *J. Chem. Phys.*, 2010, **132**, 154104.
- 13 72 G. A. Petersson, A. Bennett, T. G. Tensfeldt, M. A. Al-Laham, W. A. Shirley and J. Mantzaris, *J.*
14 *Chem. Phys.*, 1988, **89**, 2193–2218.
- 15 73 G. A. Petersson and M. A. Al-Laham, *J. Chem. Phys.*, 1991, **94**, 6081–6090.
- 16 74 T. H. Dunning Jr, *J. Chem. Phys.*, 1989, **90**, 1007–1023.
- 17 75 R. Krishnan, J. S. Binkley, R. Seeger and J. A. Pople, *J. Chem. Phys.*, 1980, **72**, 650–654.
- 18 76 A. D. Becke, *J. Chem. Phys.*, 1993, **98**, 5648–5652.
- 19 77 R. G. Parr and Y. Weitao, *Density-Functional Theory of Atoms and Molecules*, Oxford University
20 Press, 1994.
- 21 78 A. E. Reed and F. Weinhold, *J. Chem. Phys.*, 1983, **78**, 4066–4073.
- 22 79 J. P. Foster and F. Weinhold, *J. Am. Chem. Soc.*, 1980, **102**, 7211–7218.
- 23 80 Y. Shao, Z. Gan, E. Epifanovsky, A. T. B. Gilbert, M. Wormit, J. Kussmann, A. W. Lange, A.
24 Behn, J. Deng, X. Feng, D. Ghosh, M. Goldey, P. R. Horn, L. D. Jacobson, I. Kaliman, R. Z. Khaliullin,
25 T. Kuś, A. Landau, J. Liu, E. I. Proynov, Y. M. Rhee, R. M. Richard, M. A. Rohrdanz, R. P. Steele, E. J.
26 Sundstrom, H. L. W. III, P. M. Zimmerman, D. Zuev, B. Albrecht, E. Alguire, B. Austin, G. J. O. Beran,
27 Y. A. Bernard, E. Berquist, K. Brandhorst, K. B. Bravaya, S. T. Brown, D. Casanova, C.-M. Chang, Y.
28 Chen, S. H. Chien, K. D. Closser, D. L. Crittenden, M. Diefenbach, R. A. D. Jr, H. Do, A. D. Dutoi, R.
29 G. Edgar, S. Fatehi, L. Fusti-Molnar, A. Ghysels, A. Golubeva-Zadorozhnaya, J. Gomes, M. W. D.
30 Hanson-Heine, P. H. P. Harbach, A. W. Hauser, E. G. Hohenstein, Z. C. Holden, T.-C. Jagau, H. Ji, B.
31 Kaduk, K. Khistyayev, J. Kim, J. Kim, R. A. King, P. Klunzinger, D. Kosenkov, T. Kowalczyk, C. M.
32 Krauter, K. U. Lao, A. D. Laurent, K. V. Lawler, S. V. Levchenko, C. Y. Lin, F. Liu, E. Livshits, R. C.
33 Lochan, A. Luenser, P. Manohar, S. F. Manzer, S.-P. Mao, N. Mardirossian, A. V. Marenich, S. A.
34 Maurer, N. J. Mayhall, E. Neuscammann, C. M. Oana, R. Olivares-Amaya, D. P. O’Neill, J. A. Parkhill, T.
35 M. Perrine, R. Peverati, A. Prociuk, D. R. Rehn, E. Rosta, N. J. Russ, S. M. Sharada, S. Sharma, D. W.
36 Small, A. Sodt, T. Stein, D. Stück, Y.-C. Su, A. J. W. Thom, T. Tsuchimochi, V. Vanovschi, L. Vogt, O.
37 Vydrov, T. Wang, M. A. Watson, J. Wenzel, A. White, C. F. Williams, J. Yang, S. Yeganeh, S. R. Yost,

- 1 Z.-Q. You, I. Y. Zhang, X. Zhang, Y. Zhao, B. R. Brooks, G. K. L. Chan, D. M. Chipman, C. J. Cramer,
2 W. A. G. III, M. S. Gordon, W. J. Hehre, A. Klamt, H. F. S. III, M. W. Schmidt, C. D. Sherrill, D. G.
3 Truhlar, A. Warshel, X. Xu, A. Aspuru-Guzik, R. Baer, A. T. Bell, N. A. Besley, J.-D. Chai, A. Dreuw, B.
4 D. Dunietz, T. R. Furlani, S. R. Gwaltney, C.-P. Hsu, Y. Jung, J. Kong, D. S. Lambrecht, W. Liang, C.
5 Ochsenfeld, V. A. Rassolov, L. V. Slipchenko, J. E. Subotnik, T. V. Voorhis, J. M. Herbert, A. I. Krylov,
6 P. M. W. Gill and M. Head-Gordon, *Mol. Phys.*, 2015, **113**, 184–215.
- 7 81 M. J. McGrath, T. Olenius, I. K. Ortega, V. Loukonen, P. Paasonen, T. Kurtén, M. Kulmala and
8 H. Vehkamäki, *Atmos. Chem. Phys.*, 2012, **12**, 2345–2355.
- 9 82 M. J. Ezell, H. Chen, K. D. Arquero and B. J. Finlayson-Pitts, *J. Aerosol Sci.*, 2014, **78**, 30–40.
- 10 83 M. L. Dawson, V. Perraud, A. Gomez, K. D. Arquero, M. J. Ezell and B. J. Finlayson-Pitts,
11 *Atmos. Meas. Tech.*, 2014, **7**, 2733–2744.
- 12 84 Y. Liu and A. Laskin, *J. Phys. Chem. A*, 2009, **113**, 1531–1538.
- 13 85 G. Zeng, J. Kelley, J. D. Kish and Y. Liu, *J. Phys. Chem. A*, 2014, **118**, 583–591.

14

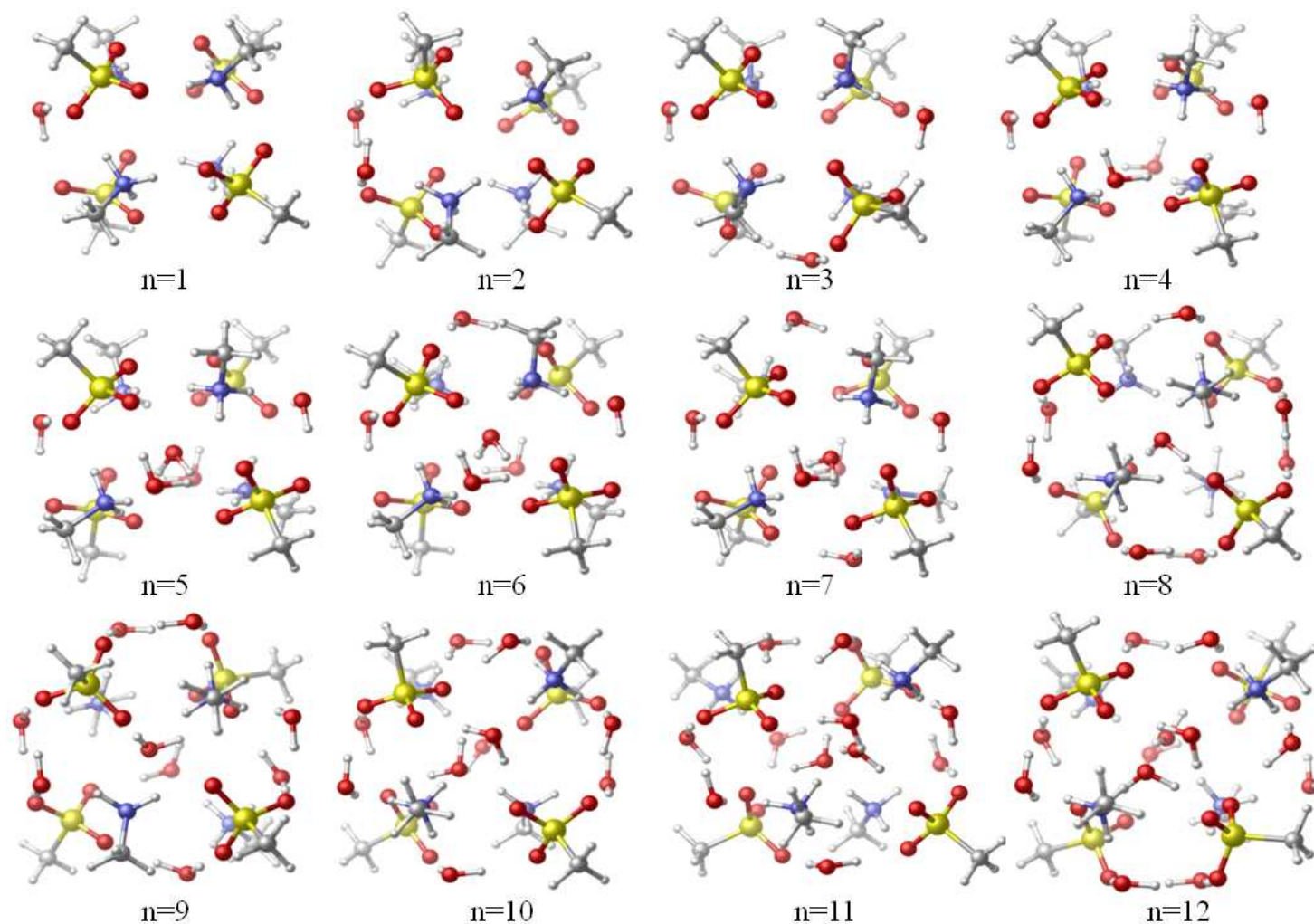


Figure 1. Structures of $(\text{MSA-MA})_4-(\text{H}_2\text{O})_n$, $n = 1$ to 12 . Yellow, red, blue, gray and white spheres represent sulfur, oxygen, nitrogen, carbon and hydrogen atoms, respectively. For a better view, all the hydrogen bonds between oxygen and hydrogen are omitted, and the molecules located on the inside of the unit cell are blurred out.

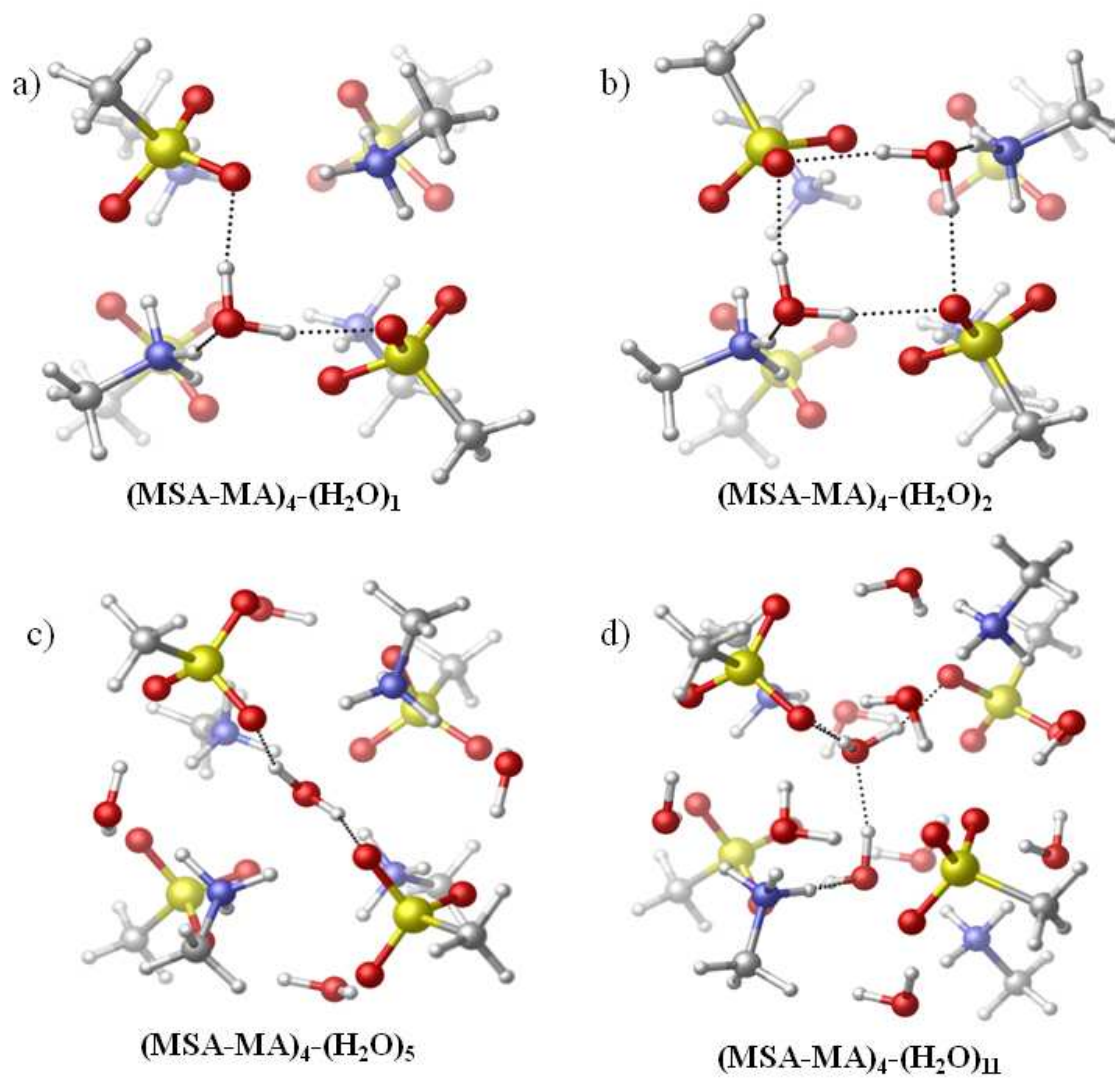


Figure 2. Different types of locations for water: a) one water on one face of the $(\text{MSA-MA})_4^-$ unit; b) two water molecules on the same face of the unit; c) one water inside the unit; d) two water molecules inside the unit.

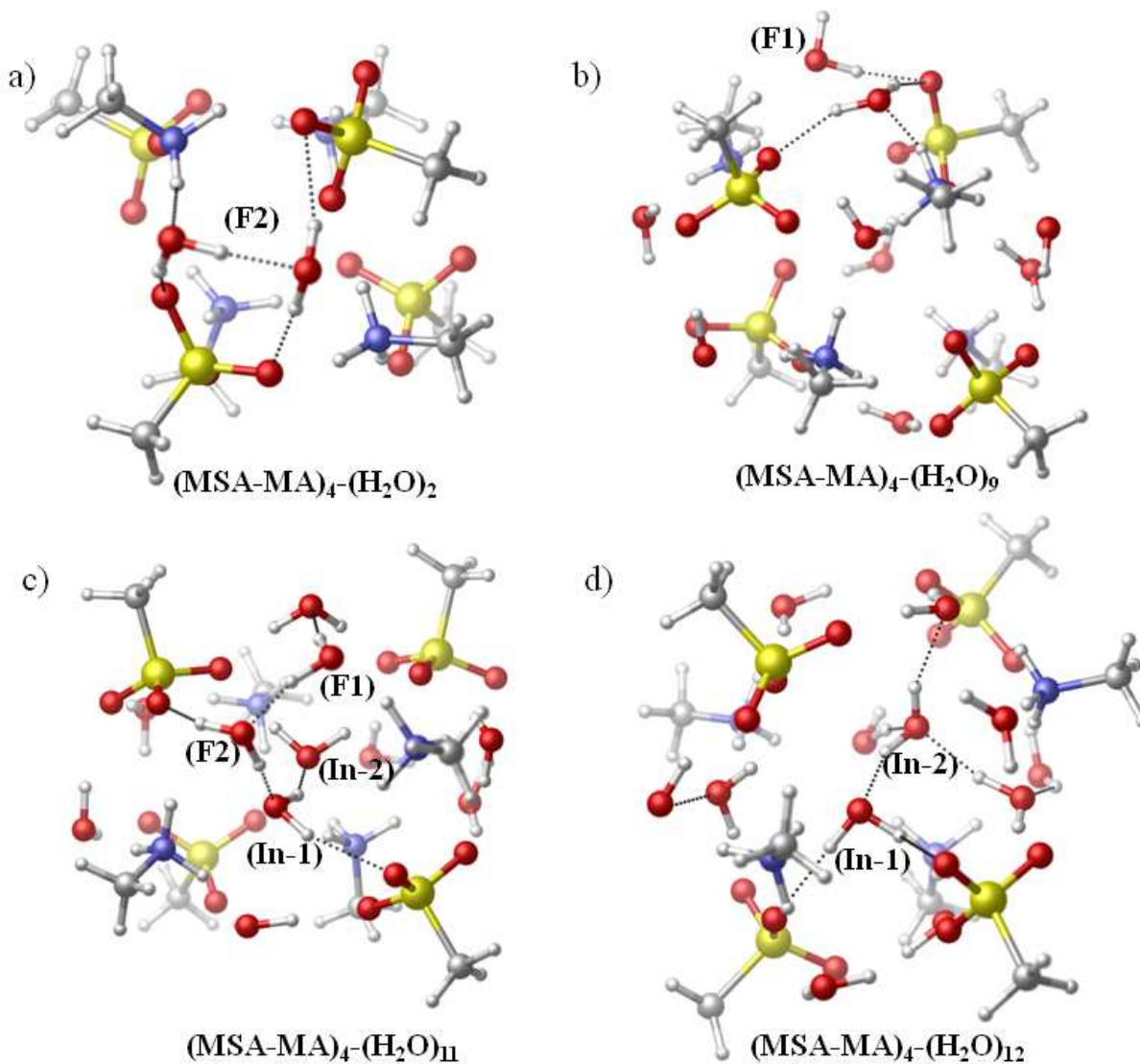


Figure 3. Structures of $(\text{MSA-MA})_4-(\text{H}_2\text{O})_n$, $n = 2, 9, 11$ and 12 clusters at 10 ps from the dynamic simulations ($T = 300$ K) at the level of BLYP-D/6-31+G(d).

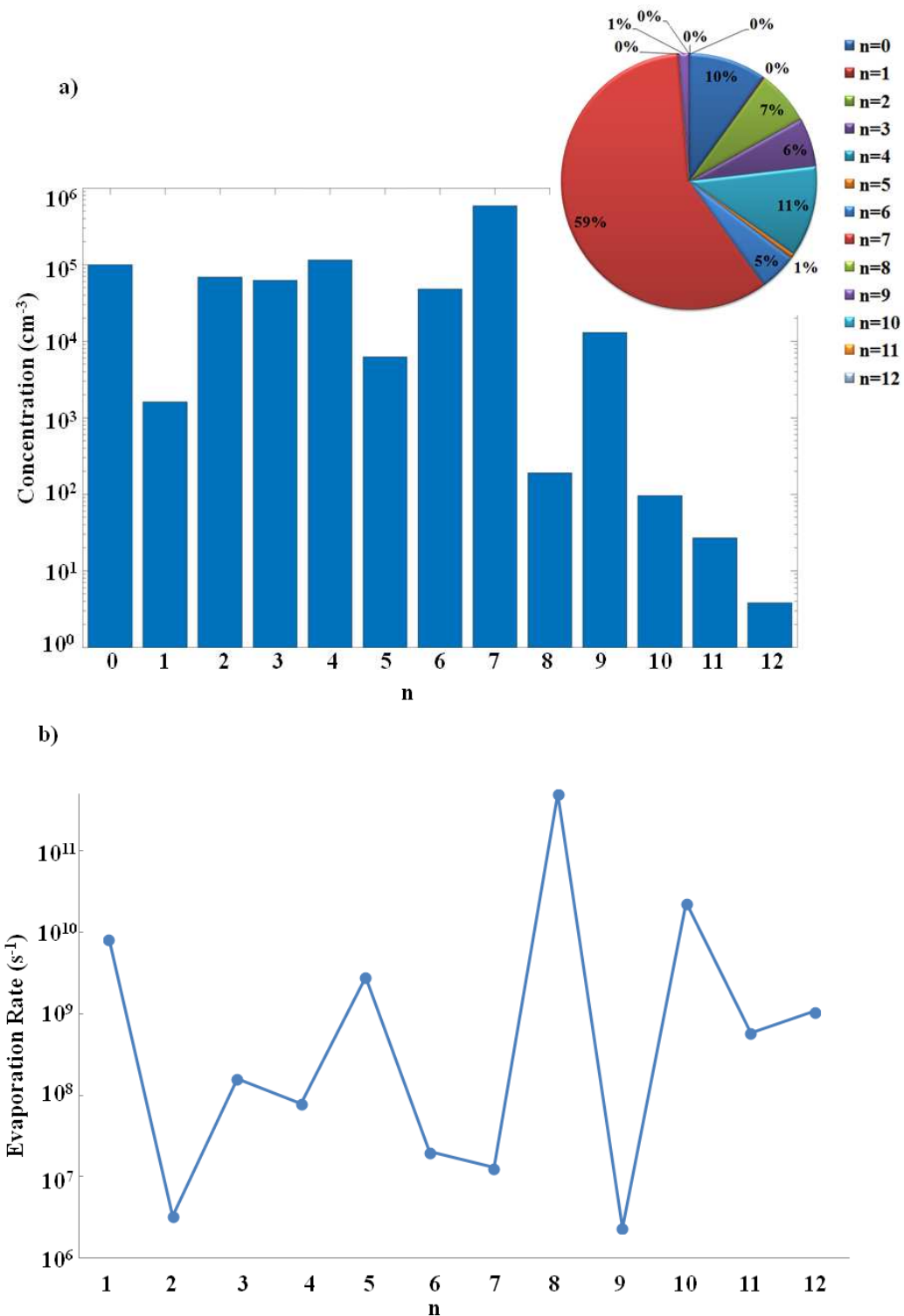


Figure 4. a) Hydrate distributions for $(\text{MSA-MA})_4\text{-(H}_2\text{O)}_n$, $n=0$ to 12 at 19% RH; b) evaporation rates of the hydrated clusters from only one single water evaporation pathway.

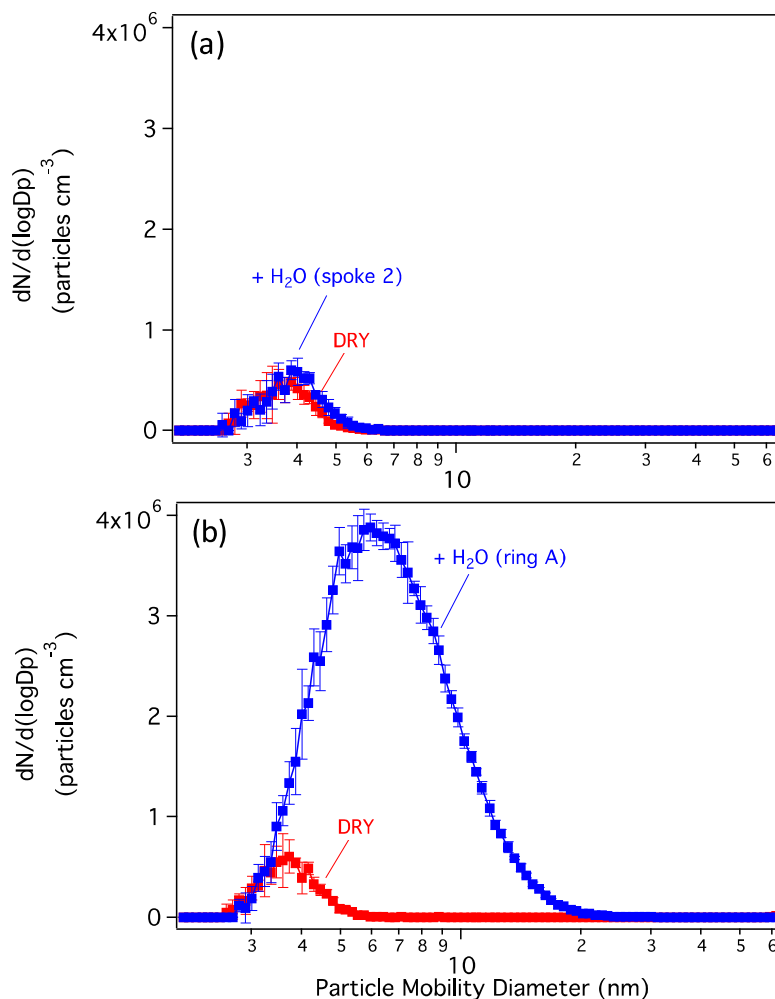
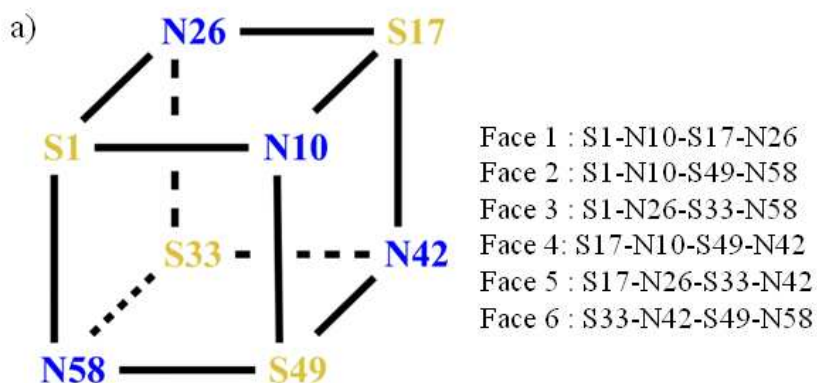


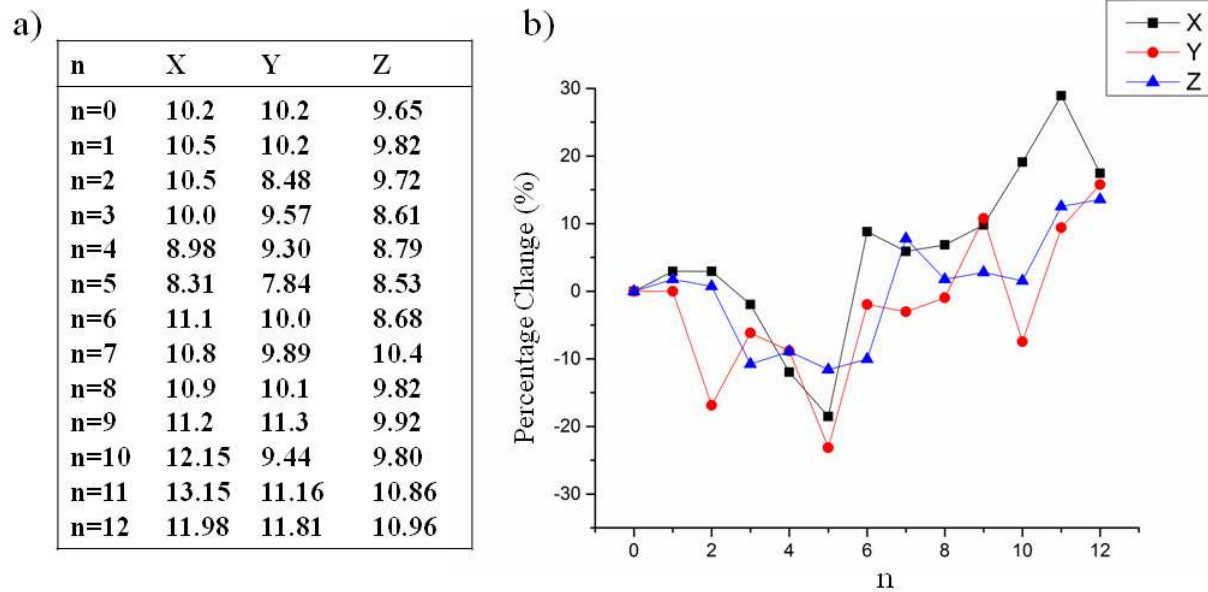
Figure 5. Size distributions of particles from the reaction of 1.7×10^{11} MSA molecules cm^{-3} (6.9 ppb) with 3.9×10^{10} MA molecules cm^{-3} (1.6 ppb) measured by SMPS (a) under dry (red trace) conditions at a reaction time of 13.9 s, and in the presence of water vapor (RH \sim 18-19%; blue trace). In the latter case, the MSA and MA reacted for 8.2 s, and then interacted with water for an additional 5.7 s; (b) under dry (red trace) conditions at a reaction time of 13.9 s, and in the presence of water added at the first ring inlet (RH \sim 18-19%; blue trace) so that MSA, MA and H₂O were all present during particle formation. The size distributions are averages of five consecutive measurements and the error bars correspond to one standard deviation.



b)

Number of water molecules	Locations of the water
$n=1$	1 (F3)
$n=2$	2 (F3)
$n=3$	1 (F3), 1 (F4), 1 (F6)
$n=4$	1 (F2), 1 (F3), 1 (F4), 1 (F5)
$n=5$	1 (F2), 1 (F3), 1 (F4), 1 (F5), In1
$n=6$	1 (F1), 1 (F2), 1 (F3), 1 (F4), 1 (F5), In1
$n=7$	1 (F1), 1 (F2), 1 (F3), 1 (F4), 1 (F5), 1 (F6), In1
$n=8$	1 (F1), 2 (F3), 2 (F4), 2 (F6), In1
$n=9$	2 (F1), 2 (F3), 2 (F4), 1 (F5), 1 (F6), In1
$n=10$	2 (F1), 2 (F3), 2 (F4), 1 (F2), 1 (F5), 1 (F6), In1
$n=11$	2 (F1), 2 (F3), 2 (F4), 1 (F2), 1 (F5), 1 (F6), In2
$n=12$	2 (F1), 2 (F3), 2 (F4), 2 (F6), 1 (F2), 1 (F5), In2

Scheme 1. a) The key skeleton of (MSA-MA)₄ with the sulfur (S) and nitrogen(N) atoms labeled along with the six defined faces; b) Locations of water in each system. F(x) means the "xth" face. **1** means only one water on one face; **2** means two water on one face; **In1** and **In2** mean one or two internal water, respectively.



Scheme 2. a) The lengths (\AA) of $(\text{MSA-MA})_4-(\text{H}_2\text{O})_n$, $n = 0$ to 12 in X, Y and Z directions. b) The percentage change (%) of the sizes of the different hydrated clusters compared to the anhydrous $(\text{MSA-MA})_4$ cluster.

Table 1. Dissociation energies with zero-point energy correction (ΔE) and Gibbs free energies (in kcal/mol) at 298 K (ΔG) of $(\text{MSA-MA})_4\text{-(H}_2\text{O)}_n$, $n = 0$ to 12 clusters at the level of BLYP-D/6-31+G(d). Complete or partial dissociation into starting reactants are considered.

	$(\text{MSA-MA})_4\text{-(H}_2\text{O)}_n \rightarrow$ 4 MSA + 4 MA + n H ₂ O		$(\text{MSA-MA})_4\text{-(H}_2\text{O)}_n \rightarrow$ $(\text{MSA-MA})_4$ + n H ₂ O	
	$\Delta E1$	$\Delta G1$	$\Delta E2$	$\Delta G2$
$n = 1$	190.6	98.80	13.84	0.58
$n = 2$	205.2	104.1	28.39	5.83
$n = 3$	218.0	107.0	41.22	8.79
$n = 4$	230.7	110.4	53.96	12.18
$n = 5$	243.1	111.7	66.32	13.47
$n = 6$	255.8	115.9	79.02	17.70
$n = 7$	270.3	120.4	93.56	22.21
$n = 8$	280.0	118.6	103.3	20.47
$n = 9$	292.9	124.2	116.2	26.01
$n = 10$	303.8	124.3	127.0	26.12
$n = 11$	314.4	126.6	137.6	28.42
$n = 12$	326.6	128.6	149.9	30.37

Table 2. Geometric mean diameter (nm) and total particle number concentration ($\# \text{ cm}^{-3}$) determined from size distribution measurements by SMPS.

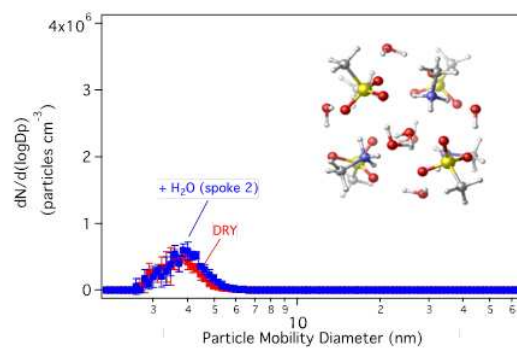
	Dry Conditions^a	Humid conditions (H₂O added at Spoke 2)^b	Humid conditions (H₂O added at Ring A)^c
Geometric Mean Diameter (nm)	3.7 (\pm 0.1)	3.9 (\pm 0.1)	6.5 (\pm 0.04)
Total Particle Number Conc. ($\# \text{ cm}^{-3}$)	$9.1 (\pm 1.3) \times 10^4$	$9.9 (\pm 1.0) \times 10^4$	$1.3 (\pm 0.6) \times 10^6$

^aMeasurements were performed at a reaction time of 13.9 s (where $t = 0$ s corresponds to ring B); error bars correspond to one standard deviation from ten replicate measurements.

^bMeasurements were performed after 8.2 s of reaction time between MSA and MA under dry conditions, and an additional 5.7 s of interaction of pre-formed particles with water (total reaction time = 13.9 s with $t = 0$ s corresponding to ring B); error bars correspond to one standard deviation from five replicate measurements.

^cMeasurements were performed at a reaction time of 13.9 s (where $t = 0$ s corresponds to ring B); Error bars correspond to one standard deviation from five replicate measurements.

TOC



Uptake of water by nanoparticles composed by methanesulfonic acid and methylamine using a combination of theoretical calculations and laboratory experiments.